

AN EFFICIENT NULLSPACE-PRESERVING SADDLE SEARCH METHOD FOR PHASE TRANSITIONS INVOLVING TRANSLATIONAL INVARIANCE*

GANG CUI[†], KAI JIANG[†], AND TIEJUN ZHOU[†]

Abstract. The bottleneck of studying phase transitions is the barrier-crossing process composed of escaping from the basin of the local minimum and finding the saddle point. Breaking the bottleneck requires designing efficient algorithms relevant to the properties of concrete phase transition. In this work, we propose an efficient nullspace-preserving saddle search (NPSS) method for a class of phase transitions involving translational invariance. These critical states in these phase transitions are usually degenerate. The NPSS overcomes the difficulty of degeneration by ensuring the ascent direction orthogonal to the kernel space of the initial minimum, then efficiently escapes from the basin and finds the saddle point. We apply the NPSS method to the phase transitions between crystals, and between crystal and quasicrystal, based on the Landau-Brazovskii and Lifshitz-Petrich free energy functionals. Numerical results show a good performance of the proposed method. Finally, we investigate an important property of the inflection point, where symmetry-breaking begins to occur and nullspace is no longer maintained.

Key words. Nullspace-preserving saddle search method, Phase transition involving translational invariance, Index-1 generalized saddle point, Generalized quadratic region, Minimum energy path, Landau free energy functional

AMS subject classifications. 37M05, 49K35, 37N30

1. Introduction. Phase transition has been a topic of great interest for many years. For systems with energy landscape, phase transition is the most probable transition path, well-known as the minimum energy paths (MEPs), between the local minima of free energy functional. Many computational approaches have been proposed to study phase transition, mainly including two classes, path-finding methods and surface-walking approaches. The former, such as the nudged elastic band approach [10, 12, 15], the string method [4, 7, 10, 25, 26], and the equal-bond-length method [6] requires a suitable initialization connecting initial and final states. The latter starts from an initial metastable state and needs a proper ascent direction to search for the transition state. Representative methods contain the gentlest ascent dynamics [8, 9], the dimer-type way [11, 42], the step and slide algorithm [22] and the high-index saddle dynamics (HiSD) method [39, 40, 41].

The bottleneck of computing phase transitions involves escaping from the basin of a local minimum and locating the relevant saddle point due to the existence of energy barriers. To break this bottleneck, we need to design efficient algorithms by exploiting the properties of concrete phase transition. In present work, we pay attention to these phase transitions involving translational invariance. Many important systems possess translational invariance including periodic crystal and quasiperiodic cases. The periodic systems have obviously translational symmetry. The quasiperiodic systems, including quasicrystals [27, 35, 36], grained boundaries [2, 13, 32], incommensu-

*Submitted to the journal's Methods and Algorithms for Scientific Computing section June 12, 2023.

Funding: This work is supported by the National Natural Science Foundation of China (12171412) and the Natural Science Foundation for Distinguished Young Scholars of Hunan Province (2021JJ10037).

[†]Hunan Key Laboratory for Computation and Simulation in Science and Engineering, Key Laboratory of Intelligent Computing and Information Processing of Ministry of Education, School of Mathematics and Computational Science, Xiangtan University, Xiangtan, Hunan, China, 411105. (Corresponding author. Kai Jiang, kaijiang@xtu.edu.cn).

rate structures [3, 29], can be embedded into high-dimensional periodic systems, thus be viewed as being translational invariance in superspace. From the perspective of energy functional these critical points (local minima, local maxima, saddle points) corresponding to ordered structures are usually *degenerate*. In other words, the Hessian of energy functional on the critical point has zero eigenvalues. The presence of nullspaces of Hessian makes escaping from the basin of local minimum difficult.

In this work, we present a nullspace-preserving saddle search (NPSS) method for phase transition with translational invariance. The NPSS method obtains an ascent direction by keeping the eigenvector directions of the Hessian orthogonal to the nullspace of the generalized local minima (GLM) in its GQR (see Definition 3.2). After escaping from this GQR, the minimum eigenvalue of its Hessian becomes negative. Then the NPSS method searches along the direction of the eigenvector corresponding to the negative eigenvalue without being affected by nullspaces. Therefore, the NPSS method can quickly escape from the basin and converge directly to the transition state with good performance in numerical computation.

We demonstrate the power of the NPSS method for phase transitions with translational invariance by the Landau-Brazovskii (LB) and the Lifshitz-Petrich (LP) models. It is also note that the NPSS can be applied to a range of models involving phase transitions with translational symmetry. In this paper, mathematical derivations presented here are exemplified using the LP model. In Section 2, we provide an overview of the LB and LP models and employ the Fourier pseudo-spectral method for spatial discretization. In Section 3, we analyze the properties of nullspaces. We present the NPSS method in Section 4. In Section 5, we apply the NPSS method to study the nucleation and phase transition between crystals, and between crystal and quasicrystal. We also compare with the HiSD method and demonstrate the superiority of the NPSS method in studying phase transitions with translational invariance. Finally, we discuss the relationship between symmetry-breaking and nullspaces on the MEP in Section 6. We find that the symmetry-breaking begins at the inflection point (IP), where the curvature changes sign on the MEP.

2. Problem formulation. Landau theory provides a powerful framework for studying the phases and phase transitions of ordered systems in both physical systems and materials [5, 24, 34]. Specifically, let the order parameter function be $u(\mathbf{r})$, the Landau models can be expressed by a free energy functional

$$(2.1) \quad E(u; \Theta) = G(u; \Theta) + F(u; \Theta),$$

where Θ represents physical parameters. $F(u)$ is the bulk energy with polynomial type formulation and $G(u)$ is the interaction energy that can contain higher-order differential operators to stabilize ordered structures.

Two classes of Landau models are considered in this paper. The first one is the LB model, which can characterize the phases and phase transitions of periodic crystals [1]. It has been applied in many different scientific fields, e.g., interfaces [37, 38], polymeric materials [28, 43]. In particular, the energy functional of the LB model is

$$(2.2) \quad E_{LB}(u) = \frac{1}{|\Omega|} \int_{\Omega} \left\{ \frac{1}{2}[(1 + \Delta)u]^2 + \frac{\tau}{2!}u^2 - \frac{\gamma}{3!}u^3 + \frac{1}{4!}u^4 \right\} d\mathbf{r},$$

where $u(\mathbf{r})$ is a real-valued function that measures the order of system. Ω is a bounded domain of the system with the volume $|\Omega|$. τ is the dimensionless reduced temperature, and γ is the phenomenological coefficient. Compared with double-well bulk

energy [33], the cubic term in the LB functional allows us to study the first-order phase transition.

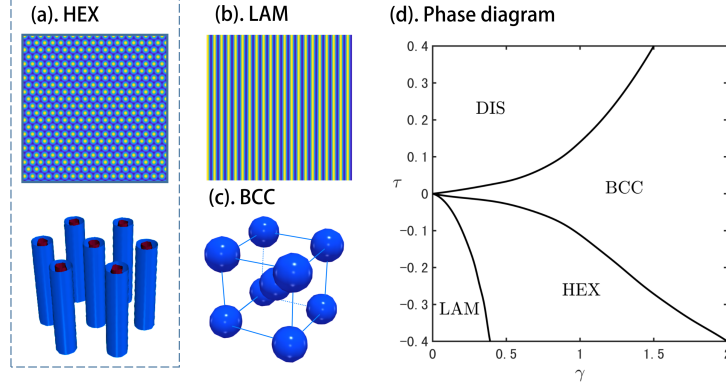


FIG. 1. *Stable ordered states and the phase diagram of the LB model. Stable ordered structures: (a). Hexagonal phase (HEX) in 2D and 3D; (b). Lamella phase (LAM); (c). Body-centered cubic spherical phase (BCC).*

The second one is the LP model, which can describe quasiperiodic structures, such as the bifrequency excited Faraday wave [19], and the stability of soft-matter quasicrystals [14, 18].

$$(2.3) \quad E_{LP}(u) = \frac{1}{|\Omega|} \int_{\Omega} \left\{ \frac{1}{2} [(q_1^2 + \Delta)(q_2^2 + \Delta)u]^2 - \frac{\varepsilon}{2} u^2 - \frac{\alpha}{3} u^3 + \frac{1}{4} u^4 \right\} d\mathbf{r},$$

where ε and α are phenomenological coefficients. q_1 and q_2 are two characteristic length scales, which is necessary to stabilize the quasicrystals. Furthermore, we impose

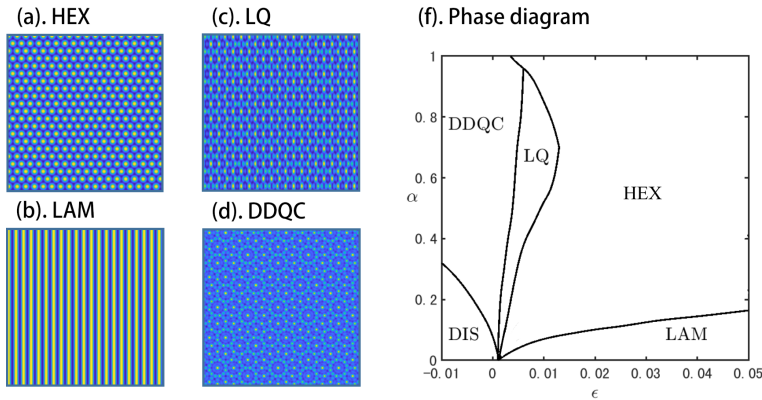


FIG. 2. *Stable ordered states and the phase diagram of the LP model with $q_1 = 1$, $q_2 = 2 \cos(\pi/12)$. Stable ordered structures: (a). HEX; (b). LAM; (c). Lamellar quasicrystal (LQ); (d). Dodecagonal quasicrystal (DDQC).*

the following mean zero condition of order parameter on the LB and LP systems,

respectively, to ensure the mass conservation

$$(2.4) \quad \frac{1}{|\Omega|} \int_{\Omega} u(\mathbf{r}) d\mathbf{r} = 0.$$

The equality constraint condition comes from the definition of the order parameter, which is the deviation from average density.

Furthermore, [Figure 1](#) and [Figure 2](#) present the phase diagrams of the LB and LP models, respectively, only involving ordered structures considered in this paper. More sophisticated phase diagrams can refer to [\[20, 39\]](#).

2.1. Fourier pseudo-spectral method discretization. In this section, we introduce the Fourier pseudo-spectral method to discretize the LP energy functional. For an n -dimensional periodic order parameter $u(\mathbf{r})$, $\mathbf{r} \in \Omega := \mathbb{R}^n / \mathbf{A}\mathbb{Z}^n$, where $\mathbf{A} = (\mathbf{a}_1, \mathbf{a}_2, \dots, \mathbf{a}_n) \in \mathbb{R}^{n \times n}$ is the primitive Bravais lattice. The primitive reciprocal lattice $\mathbf{B} = (\mathbf{b}_1, \mathbf{b}_2, \dots, \mathbf{b}_n) \in \mathbb{R}^{n \times n}$, satisfies the dual relation

$$(2.5) \quad \mathbf{A}\mathbf{B}^T = 2\pi\mathbf{I}.$$

The order parameter $u(\mathbf{r})$ can be expanded as

$$(2.6) \quad u(\mathbf{r}) = \sum_{\mathbf{k} \in \mathbb{Z}^n} \hat{u}(\mathbf{k}) e^{i(\mathbf{B}\mathbf{k})^T \mathbf{r}}, \quad \mathbf{r} \in \Omega,$$

where the Fourier coefficient

$$(2.7) \quad \hat{u}(\mathbf{k}) = \frac{1}{|\Omega|} \int_{\Omega} u(\mathbf{r}) e^{-i(\mathbf{B}\mathbf{k})^T \mathbf{r}} d\mathbf{r}.$$

We define the discrete grid set as

$$(2.8) \quad \Omega_N = \left\{ (r_{1,j_1}, \dots, r_{n,j_n}) = \mathbf{A}(j_1/N, \dots, j_n/N)^T, j_i = 0, \dots, N-1, i = 1, \dots, n \right\},$$

where the number of elements of Ω_N is $M = N^n$. Denote the grid periodic function space $\mathcal{G}_N = \{f : \Omega_N \mapsto \mathbb{C}, f \text{ is periodic}\}$. For any periodic grid functions $f, g \in \mathcal{G}_N$, we define the ℓ^2 -inner product as

$$(2.9) \quad \langle f, g \rangle = \frac{1}{M} \sum_{\mathbf{r}_j \in \Omega_N} f(\mathbf{r}_j) \bar{g}(\mathbf{r}_j).$$

The discrete reciprocal space is

$$(2.10) \quad \mathbb{K}_N^n = \{\mathbf{k} = (k_j)_{j=1}^n \in \mathbb{Z}^n : -N/2 \leq k_j < N/2\}.$$

For $\mathbf{k} \in \mathbb{Z}^n$ and $\mathbf{l} \in \mathbb{Z}^n$, we have the discrete orthogonality

$$(2.11) \quad \langle e^{i(\mathbf{B}\mathbf{k})^T \mathbf{r}_j}, e^{i(\mathbf{B}\mathbf{l})^T \mathbf{r}_j} \rangle = \begin{cases} 1, & \mathbf{k} = \mathbf{l} + N\mathbf{m}, \mathbf{m} \in \mathbb{Z}^n, \\ 0, & \text{otherwise.} \end{cases}$$

Then the discrete Fourier coefficients of $u(\mathbf{r})$ in Ω_N can be represented as

$$(2.12) \quad \hat{u}(\mathbf{k}) = \langle u(\mathbf{r}_j), e^{i(\mathbf{B}\mathbf{k})^T \mathbf{r}_j} \rangle = \frac{1}{M} \sum_{\mathbf{r}_j \in \Omega_N} u(\mathbf{r}_j) e^{-i(\mathbf{B}\mathbf{k})^T \mathbf{r}_j}, \quad \mathbf{k} \in \mathbb{K}_N^n.$$

Let $U = (u_1, u_2, \dots, u_M) \in \mathbb{R}^M$, where $u_j = u(\mathbf{r}_j)$, $1 \leq j \leq M$. Denote $\mathcal{F}_M \in \mathbb{C}^{M \times M}$ as the discretized Fourier transformation matrix, then we have the discrete order parameter $\hat{U} = \mathcal{F}_M U$ in reciprocal space. The discretized energy function (2.3) is

$$(2.13) \quad E_{\mathbf{k}}(\hat{U}) = G_{\mathbf{k}}(\hat{U}) + F_{\mathbf{k}}(\hat{U}),$$

where $G_{\mathbf{k}}$ and $F_{\mathbf{k}}$ are the discretized interaction and bulk energies,

$$(2.14) \quad \begin{aligned} G_{\mathbf{k}}(\hat{U}) &= \frac{c}{2} \sum_{\mathbf{k}_1 + \mathbf{k}_2 = 0} [q_1^2 - (\mathbf{B}\mathbf{k})^\top (\mathbf{B}\mathbf{k})]^2 [q_2^2 - (\mathbf{B}\mathbf{k})^\top (\mathbf{B}\mathbf{k})]^2 \hat{U}(\mathbf{k}_1) \hat{U}(\mathbf{k}_2), \\ F_{\mathbf{k}}(\hat{U}) &= -\frac{\varepsilon}{2} \sum_{\mathbf{k}_1 + \mathbf{k}_2 = 0} \hat{U}(\mathbf{k}_1) \hat{U}(\mathbf{k}_2) - \frac{\alpha}{3} \sum_{\mathbf{k}_1 + \mathbf{k}_2 + \mathbf{k}_3 = 0} \hat{U}(\mathbf{k}_1) \hat{U}(\mathbf{k}_2) \hat{U}(\mathbf{k}_3) \\ &\quad + \frac{1}{4} \sum_{\mathbf{k}_1 + \mathbf{k}_2 + \mathbf{k}_3 + \mathbf{k}_4 = 0} \hat{U}(\mathbf{k}_1) \hat{U}(\mathbf{k}_2) \hat{U}(\mathbf{k}_3) \hat{U}(\mathbf{k}_4), \end{aligned}$$

and $\mathbf{k}_j \in \mathbb{K}_N^n$. The nonlinear terms $F_{\mathbf{k}}$ can be obtained by the FFT after being calculated in the n -dimensional physical space. Moreover, the mass conservation constraint (2.4) is discretized as

$$(2.15) \quad e_1^\top \hat{U} = 0,$$

where $e_1 = (1, 0, \dots, 0)^\top \in \mathbb{R}^M$. Therefore, we obtain the following finite-dimensional minimization problem to obtain various ordered structures

$$(2.16) \quad \min_{\hat{U} \in \mathbb{C}^N} E_{\mathbf{k}}(\hat{U}) = G_{\mathbf{k}}(\hat{U}) + F_{\mathbf{k}}(\hat{U}) \quad \text{s.t.} \quad e_1^\top \hat{U} = 0.$$

For simplicity, we omit the subscription in $G_{\mathbf{k}}$ and $F_{\mathbf{k}}$ in the following context. According to (2.14), we have

$$(2.17) \quad \nabla G(\hat{U}) = D\hat{U}, \nabla F(\hat{U}) = \mathcal{F}_M^{-1} \Lambda \mathcal{F}_M \hat{U},$$

$$(2.18) \quad \nabla^2 G(\hat{U}) = D, \nabla^2 F(\hat{U}) = \mathcal{F}_M^{-1} \Lambda^{(\prime)} \mathcal{F}_M,$$

where D is a diagonal matrix with non-negative entries $c[q_1^2 - (\mathbf{B}\mathbf{k})^\top (\mathbf{B}\mathbf{k})]^2 [q_2^2 - (\mathbf{B}\mathbf{k})^\top (\mathbf{B}\mathbf{k})]^2$ and $\Lambda, \Lambda^{(\prime)} \in \mathbb{R}^{M \times M}$ are also diagonal matrices but related to \hat{U} .

3. Analysis of nullspace. The nullspace of the Hessian on the MEP can affect the performance of saddle point search methods when studying phase transitions with translational invariance. In this section, we show the properties of nullspaces by theoretical analysis and numerical observations.

Firstly, we rewrite the energy function (2.13) as

$$(3.1) \quad E(U) = G(U) + F(U),$$

and the gradient and Hessian of $E(U)$ can be written as

$$(3.2) \quad \nabla E(U) = \mathcal{F}_M (\nabla G(\hat{U}) + \nabla F(\hat{U})) = \mathcal{F}_M D \hat{U} + \Lambda \mathcal{F}_M \hat{U} = \mathcal{F}_M D \mathcal{F}_M^{-1} U + \Lambda U,$$

$$(3.3) \quad H(U) = \mathcal{F}_M (\nabla^2 G(\hat{U}) + \nabla^2 F(\hat{U})) = \mathcal{F}_M (D + \Lambda^{(\prime)} \mathcal{F}_M) = \mathcal{F}_M D \mathcal{F}_M^{-1} + \Lambda^{(\prime)},$$

where $\Lambda = \text{diag}(-\varepsilon - \alpha U + U^2)$, $\Lambda^{(\prime)} = \text{diag}(-\varepsilon - 2\alpha U + 3U^2)$.

Now we discuss the critical points of degenerate and non-degenerate cases. For an energy function E represented by (3.1), a critical point of E satisfies $\nabla E(U) = 0$. To distinguish mathematically different critical points, we introduce the Morse index [31]. The Morse index of a non-degenerate critical point U is equal to the number of negative eigenvalues of $H(U)$. For degenerate problems, we can extend the definition of the Morse index to depict critical points.

DEFINITION 3.1. (1). *Generalized Morse index.* For a degenerate or non-degenerate critical point, the generalized Morse index is the number of negative eigenvalues of its Hessian.

(2). *Generalized critical point.* A critical point is called the index- k generalized saddle point (GSP) if its generalized Morse index is k ($k > 0$). If $k = 1$, it is an index-1 GSP, characterized as the transition state. If $k = 0$, it is a GLM.

Notably, the Morse index is a special case of the generalized Morse index. Similarly, we define the GQR of the critical points,

DEFINITION 3.2. For a generalized critical point, its neighbourhood is called the GQR if the generalized Morse index of all interior points is the same as that of the generalized critical point.

The quadratic region of a non-degenerate critical point has been mentioned in [23]. Moreover, we define unstable, stable subspaces and nullspace of $H(U)$ as

$$(3.4) \quad \mathcal{W}^u(U) = \text{span}_{\mathbb{R}}\{\mathbf{v}_1^u, \dots, \mathbf{v}_{l_u}^u\},$$

$$(3.5) \quad \mathcal{W}^s(U) = \text{span}_{\mathbb{R}}\{\mathbf{v}_1^s, \dots, \mathbf{v}_{l_s}^s\},$$

$$(3.6) \quad \mathcal{W}^k(U) = \text{span}_{\mathbb{R}}\{\mathbf{v}_1^k, \dots, \mathbf{v}_{l_k}^k\},$$

where $\{\mathbf{v}_1^u, \dots, \mathbf{v}_{l_u}^u\}$, $\{\mathbf{v}_1^s, \dots, \mathbf{v}_{l_s}^s\}$ and $\{\mathbf{v}_1^k, \dots, \mathbf{v}_{l_k}^k\} \subset \mathbb{R}^M$ are eigenvectors of $H(U)$ corresponding to negative, positive, and zero eigenvalues, respectively. $l_u + l_s + l_k = M$. According to the primary decomposition theorem [21], \mathbb{R}^M can be decomposed as

$$(3.7) \quad \mathbb{R}^M = \mathcal{W}^u(U) \oplus \mathcal{W}^s(U) \oplus \mathcal{W}^k(U),$$

where the dimensions l_u , l_s , l_k of subspaces $\mathcal{W}^u(U)$, $\mathcal{W}^s(U)$, $\mathcal{W}^k(U)$ depend on the location of U on the energy surface.

3.1. Translational invariance and nullspace. Critical points involved in phase transitions with translational invariance generally correspond to periodic or quasi-periodic phases. Although quasicrystals lack translational invariance in physical space, they can be embedded in higher-dimensional periodic systems. Thus we can analyze the properties of these phases uniformly in suitable periodic systems. For a non-zero periodic critical point, we discuss the relationship between nullspace's dimension of its Hessian and translational invariance in this subsection.

PROPOSITION 3.3. Let U be a n -dimensional non-zero periodic critical point of E (3.1), then $\dim \mathcal{W}^k(U) \geq n$.

Proof. According to (3.2), the critical point U satisfies

$$(3.8) \quad \nabla E(U) = \mathcal{F}_M D\mathcal{F}_M^{-1}U + \Lambda U = 0.$$

Define the discrete derivative operator as

$$(3.9) \quad \mathcal{F}_M K_j \mathcal{F}_M^{-1}, \quad j = 1, 2, \dots, n,$$

where K_j is a diagonal matrix, the diagonal elements relate to $i \cdot k_j$. k_j is the j -th component of spectral point \mathbf{k} and i is the imaginary unit.

Acting operator (3.9) on (3.8) leads to

$$(3.10) \quad \mathcal{F}_M K_j D \mathcal{F}_M^{-1} U + \mathcal{F}_M K_j \mathcal{F}_M^{-1} \Lambda U = \mathcal{F}_M K_j D \hat{U} + \mathcal{F}_M K_j \widehat{\Lambda U} = 0.$$

Let

$$(3.11) \quad \mathbf{v}_j = \mathcal{F}_M K_j \hat{U} \in \mathbb{R}^M, \quad j = 1, 2, \dots, n.$$

By acting the Hessian (3.3) on \mathbf{v}_j ,

$$(3.12) \quad \begin{aligned} (\mathcal{F}_M D \mathcal{F}_M^{-1} + \Lambda^{(\prime)}) \mathbf{v}_j &= (\mathcal{F}_M D \mathcal{F}_M^{-1} + \Lambda^{(\prime)}) \mathcal{F}_M K_j \hat{U} \\ &= \mathcal{F}_M D \mathcal{F}_M^{-1} \mathcal{F}_M K_j \hat{U} + \Lambda^{(\prime)} \mathcal{F}_M K_j \hat{U} \\ &= \mathcal{F}_M D K_j \hat{U} + \Lambda^{(\prime)} \mathcal{F}_M K_j \hat{U} \\ &\stackrel{(*)}{=} \mathcal{F}_M K_j D \hat{U} + \Lambda^{(\prime)} \mathcal{F}_M K_j \hat{U}, \end{aligned}$$

where $(*)$ holds because D and K_j are diagonal, $D K_j = K_j D$.

For brevity, we write $P = (p_s)_{s=1}^M = \mathcal{F}_M K_j \widehat{\Lambda U}$ and $Q = (q_s)_{s=1}^M = \Lambda^{(\prime)} \mathcal{F}_M K_j \hat{U}$. Let \mathbf{k} , \mathbf{k}_1 , \mathbf{k}_2 , $\mathbf{k}_3 \in \mathbb{K}_N^n$, and k_j , $k_{1,j}$, $k_{2,j}$, $k_{3,j}$ be the j -th component of them, respectively. $\mathbf{r}_s = (r_1, \dots, r_n) \in \Omega_N$ is the coordinate of the s -th element in U . Denote p_s and q_s as the s -th element of P, Q . For $s = 1, \dots, M$, p_s and q_s can be written as

$$(3.13) \quad \begin{aligned} p_s &= -\varepsilon \sum_{\mathbf{k} \in \mathbb{K}_N^n} i k_j \hat{u}(\mathbf{k}) e^{i \mathbf{k} \mathbf{r}_s} - \alpha \sum_{\mathbf{k} \in \mathbb{K}_N^n} i k_j \sum_{\mathbf{k}_1 + \mathbf{k}_2 = \mathbf{k}} \hat{u}(\mathbf{k}_1) \hat{u}(\mathbf{k}_2) e^{i \mathbf{k} \mathbf{r}_s} \\ &\quad + \sum_{\mathbf{k} \in \mathbb{K}_N^n} i k_j \sum_{\mathbf{k}_1 + \mathbf{k}_2 + \mathbf{k}_3 = \mathbf{k}} \hat{u}(\mathbf{k}_1) \hat{u}(\mathbf{k}_2) \hat{u}(\mathbf{k}_3) e^{i \mathbf{k} \mathbf{r}_s} \\ &= -\varepsilon \sum_{\mathbf{k} \in \mathbb{K}_N^n} i k_j \hat{u}(\mathbf{k}) e^{i \mathbf{k} \mathbf{r}_s} - \alpha \sum_{\mathbf{k} \in \mathbb{K}_N^n} i (k_{1,j} + k_{2,j}) \sum_{\mathbf{k}_1 + \mathbf{k}_2 = \mathbf{k}} \hat{u}(\mathbf{k}_1) \hat{u}(\mathbf{k}_2) e^{i \mathbf{k} \mathbf{r}_s} \\ &\quad + \sum_{\mathbf{k} \in \mathbb{K}_N^n} i (k_{1,j} + k_{2,j} + k_{3,j}) \sum_{\mathbf{k}_1 + \mathbf{k}_2 + \mathbf{k}_3 = \mathbf{k}} \hat{u}(\mathbf{k}_1) \hat{u}(\mathbf{k}_2) \hat{u}(\mathbf{k}_3) e^{i \mathbf{k} \mathbf{r}_s} \\ &\stackrel{(\#)}{=} -\varepsilon \sum_{\mathbf{k} \in \mathbb{K}_N^n} i k_j \hat{u}(\mathbf{k}) e^{i \mathbf{k} \mathbf{r}_s} - 2\alpha \sum_{\mathbf{k} \in \mathbb{K}_N^n} \sum_{\mathbf{k}_1 + \mathbf{k}_2 = \mathbf{k}} i k_{1,j} \hat{u}(\mathbf{k}_1) \hat{u}(\mathbf{k}_2) e^{i \mathbf{k} \mathbf{r}_s} \\ &\quad + 3 \sum_{\mathbf{k} \in \mathbb{K}_N^n} \sum_{\mathbf{k}_1 + \mathbf{k}_2 + \mathbf{k}_3 = \mathbf{k}} i k_{1,j} \hat{u}(\mathbf{k}_1) \hat{u}(\mathbf{k}_2) \hat{u}(\mathbf{k}_3) e^{i \mathbf{k} \mathbf{r}_s}, \end{aligned}$$

$$(3.14) \quad \begin{aligned} q_s &= [-\varepsilon - 2\alpha \sum_{\mathbf{k} \in \mathbb{K}_N^n} \hat{u}(\mathbf{k}) e^{i \mathbf{k} \mathbf{r}_s} \\ &\quad + 3 \sum_{\mathbf{k} \in \mathbb{K}_N^n} \sum_{\mathbf{k}_2 + \mathbf{k}_3 = \mathbf{k}} \hat{u}(\mathbf{k}_2) \hat{u}(\mathbf{k}_3) e^{i \mathbf{k} \mathbf{r}_s}] \sum_{\mathbf{k} \in \mathbb{K}_N^n} i k_j \hat{u}(\mathbf{k}) e^{i \mathbf{k} \mathbf{r}_s} \\ &= -\varepsilon \sum_{\mathbf{k} \in \mathbb{K}_N^n} i k_j \hat{u}(\mathbf{k}) e^{i \mathbf{k} \mathbf{r}_s} - 2\alpha \sum_{\mathbf{k} \in \mathbb{K}_N^n} \sum_{\mathbf{k}_1 + \mathbf{k}_2 = \mathbf{k}} i k_{1,j} \hat{u}(\mathbf{k}_1) \hat{u}(\mathbf{k}_2) e^{i \mathbf{k} \mathbf{r}_s} \\ &\quad + 3 \sum_{\mathbf{k} \in \mathbb{K}_N^n} \sum_{\mathbf{k}_1 + \mathbf{k}_2 + \mathbf{k}_3 = \mathbf{k}} i k_{1,j} \hat{u}(\mathbf{k}_1) \hat{u}(\mathbf{k}_2) \hat{u}(\mathbf{k}_3) e^{i \mathbf{k} \mathbf{r}_s}, \end{aligned}$$

where (#) holds because $k_{1,j}, k_{2,j}, k_{3,j}$ are symmetric.

From (3.13) and (3.14), we have $p_s = q_s$. Therefore,

$$(3.15) \quad \mathcal{F}_M K_j \widehat{\Lambda \hat{U}} = \Lambda^{(\prime)} \mathcal{F}_M K_j \hat{U}.$$

Combined with (3.10) and (3.12), we have

$$(3.16) \quad (\mathcal{F}_M D \mathcal{F}_M^{-1} + \Lambda^{(\prime)}) \mathbf{v}_j = 0,$$

then we can conclude that $\mathbf{v}_j \in \mathcal{W}^k(U), j = 1, \dots, n$.

Next, we consider the dimension of $\text{span}\{\mathbf{v}_1, \mathbf{v}_2, \dots, \mathbf{v}_n\}$. Denote $A \circ B = [a_{ij} b_{ij}]$ as the Hadamard product, where $A = [a_{ij}]$ and $B = [a_{ij}]$ are two matrices with the same order. Then

$$(3.17) \quad \mathcal{F}_M^{-1} \mathbf{v}_j = K_j \hat{U} = i \tilde{\mathbf{k}}_j \circ \hat{U}, \quad j = 1, 2, \dots, n,$$

where $\tilde{\mathbf{k}}_j(s) = K_j(ss)$. Define $\mathbf{v} = \sum_{j=1}^n \alpha_j \mathbf{v}_j$ with $\boldsymbol{\alpha} = (\alpha_1, \dots, \alpha_n)^\top \in \mathbb{R}^n$. $\mathcal{F}_M^{-1} \mathbf{v}$ are give by

$$(3.18) \quad \begin{aligned} \mathcal{F}_M^{-1} \mathbf{v} &= (\mathcal{F}_M^{-1} \mathbf{v}_1, \dots, \mathcal{F}_M^{-1} \mathbf{v}_n) \boldsymbol{\alpha} \\ &= i(\tilde{\mathbf{k}}_1 \circ \hat{U}, \dots, \tilde{\mathbf{k}}_n \circ \hat{U}) \boldsymbol{\alpha} \\ &= i\hat{U} \circ (\tilde{\mathbf{k}}_1, \dots, \tilde{\mathbf{k}}_n) \boldsymbol{\alpha}. \end{aligned}$$

Denote $\mathbf{k} = (k_1, \dots, k_n) \in \mathbb{K}_N^n$ as any row of $(\tilde{\mathbf{k}}_1, \dots, \tilde{\mathbf{k}}_n)$, and $\mathcal{K}(U) := \{\mathbf{k} \in \mathbb{K}_N^n : \hat{U}(\mathbf{k}) \neq 0\}$, we have

$$(3.19) \quad \mathbf{v} = 0 \iff \mathcal{F}_M^{-1} \mathbf{v} = 0 \text{ for all } \mathbf{k} \in \mathbb{K}_N^n \iff \mathbf{k} \cdot \boldsymbol{\alpha} = 0 \text{ for all } \mathbf{k} \in \mathcal{K}(U),$$

implying that the dimension of $\text{span}\{\mathbf{v}_1, \mathbf{v}_2, \dots, \mathbf{v}_n\}$ is exactly the dimension of $\mathcal{K}(U)$. If U is a non-zero periodic state on Ω_N , then we know that $\dim \mathcal{K}(U) = n$, hence $\dim \mathcal{W}^k(U) \geq n$. \square

REMARK 3.1. For an n -dimensional non-zero periodic critical point U , we have $\dim \mathcal{W}^k(U) \geq n$. However, numerous numerical experiments show that $\dim \mathcal{W}^k(U) = n$. Here, we present an example in Table 1.

TABLE 1
Seven numerical smallest eigenvalues of $H(U)$ corresponding to stable ordered structures in LP model with $\varepsilon = 0.05, \alpha = 1$.

HEX	-6.53e-17	-1.26e-17	5.57e-4	5.567e-4	5.58e-4	5.58e-4	1.11e-3
LQ	-9.50e-16	-1.28e-17	1.82e-17	2.57e-4	2.57e-4	5.80e-4	5.80e-4
DDQC	-5.42e-17	-5.99e-17	-1.44e-17	-7.67e-18	1.69e-3	1.69e-3	1.69e-3

HEX is a 2-dimensional periodic structure, and 2-dimensional LQ, DDQC can be embedded into 3- and 4- dimensional periodic systems, respectively. From Table 1, HEX, LQ, and DDQC have 2, 3, and 4 zero eigenvalues, respectively. Thus we posit that $\dim \mathcal{W}^k(U) = n$, despite the definitive proof for this assertion remains open. Consequently, we can directly obtain the nullspace at U by using (3.11) without numerical computation.

3.2. Impact of nullspace on escaping from basin. In ordered phase transition, our target is to locate an index-1 GSP from a GLM. However, due to the degeneracy of GLMs, the presence of nullspace hinder the escape from the basin of attraction. Therefore we analyze the effect of nullspace on escaping from the basin in this subsection.

For a non-zero periodic GLM \tilde{U} , the subspaces of its Hessian include $\mathcal{W}^s(\tilde{U})$ and $\mathcal{W}^k(\tilde{U})$. The energy remains stable when perturbed in $\mathcal{W}^k(\tilde{U})$ at \tilde{U} .

PROPOSITION 3.4. *Let \tilde{U} be a non-zero periodic GLM of $E(U)$. For any given $\epsilon > 0$, and any $\delta U \in \mathcal{W}^k(\tilde{U})$ satisfies $\|\delta U\|_{\ell^2} < \epsilon$, we have $|E(\tilde{U} + \delta U) - E(\tilde{U})| < o(\epsilon^2)$.*

Proof. Since \tilde{U} is a GLM, we have $\nabla E(\tilde{U}) = 0$. For any $\delta U \in \mathcal{W}^k(\tilde{U})$, we have $\langle \delta U, H(\tilde{U})\delta U \rangle = 0$. We employ the Taylor expansion of $E(U)$ at \tilde{U} ,

$$(3.20) \quad \begin{aligned} E(\tilde{U} + \delta U) &= E(\tilde{U}) + \nabla E(\tilde{U})\delta U + \frac{\langle \delta U, H(\tilde{U})\delta U \rangle}{2!} + o(\|\delta U\|_{\ell^2}^2) \\ &= E(\tilde{U}) + o(\|\delta U\|_{\ell^2}^2), \end{aligned}$$

where $\delta U \in \mathcal{W}^k(\tilde{U})$ satisfies $\|\delta U\|_{\ell^2} < \epsilon$. Then we have $|E(\tilde{U} + \delta U) - E(\tilde{U})| \leq o(\epsilon^2)$. \square

Proposition 3.4 indicates that the energy remains almost unchanged by a minor perturbation of the nullspace for the GLM. For phase transitions with translational invariance, existing surface-walking methods that search for saddle points along the eigenvector \mathbf{v} linked to the smallest eigenvalue, such as the gentlest ascent dynamics and dimer-type methods, could be challenging to escape from the attraction basin [39]. Since $\mathbf{v} \in \mathcal{W}^k(\tilde{U})$, a slight movement along \mathbf{v} does not result in an increase in energy value at the GLM \tilde{U} . In order to avoid being trapped in a basin, we introduce the NPSS method in **Section 4**, which ensures that the search direction is always upward.

4. Nullspace-preserving saddle search method. In this section, we propose the NPSS method to find the index-1 GSP from an initial GLM on the energy surface. For a state sufficiently close to the GLM, nullspaces of its Hessian can be approximated by nullspaces of the Hessian of the GLM. We define a nullspace-preserving neighbourhood of the GLM as where the nullspace of states in this region is nearly equal to its nullspace. As shown in **Figure 3**, for a state in the nullspace-preserving neighbourhood of the GLM, we adopt a surrogate model to approximate the real one. Specifically, to update the ascent subspace, we approximate the nullspace of this state by that of the GLM and keep the ascent direction orthogonal to the nullspace of the GLM. After leaving the nullspace-preserving neighbourhood of the GLM, we continue to use the surrogate model until escaping from the GQR of the GLM, even though the nullspaces of the current state and that of the GLM are no longer approximately equivalent. Therefore, we divide the NPSS method into two stages. In stage I, the NPSS method keeps the ascent direction orthogonal to the nullspace of the GLM. In stage II, it searches along the eigenvector corresponding to the minimum eigenvalue. The mathematical description of the NPSS algorithm is given below.

4.1. Stage I : Escape from basin. Let $U^{(0)}$ represent the GLM, we consider a state U in the nullspace-preserving neighbourhood of $U^{(0)}$, whose Hessian's subspaces contain $\mathcal{W}^k(U)$ and $\mathcal{W}^s(U)$. Admittedly, we can approximate $\mathcal{W}^k(U)$ by $\mathcal{W}^k(U^{(0)})$. A relatively easy way to leave the GLM's basin is along the eigenvector \mathbf{v} of the smallest positive eigenvalue, which provides the gentlest ascent direction. We use this eigenvector to define the ascent space $V = \text{span}\{\mathbf{v}\}$ and denote its orthogonal

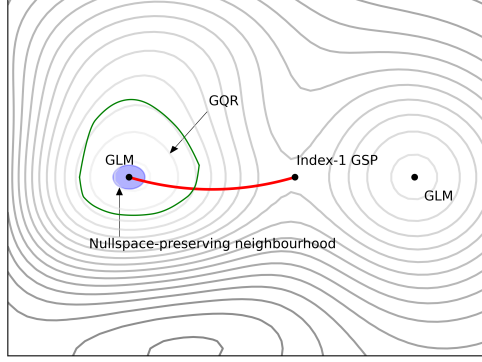


FIG. 3. Illustration of the energy surface. The evolution path is shown as a red curve. The GLM, and index-1 GSP are represented by black points on the MEP. The blue region represents the nullspace-preserving neighbourhood of the GLM, while the green curve is the boundary of the GQR of the GLM.

complement as V^\perp . The negative chemical potential is $T(U) = -\nabla E(U)$, and \mathcal{P}_V is the orthogonal projection operator on a subspace V . To escape from the basin efficiently, we take $-\mathcal{P}_V T(U)$ as an ascent direction on the subspace V , and $\mathcal{P}_{V^\perp} T(U)$ as a descent direction on the subspace V^\perp . Escaping from the basin can be achieved by the gradient-type dynamics

$$(4.1) \quad \dot{U} = \beta_1 (-\mathcal{P}_V T(U)) + \beta_2 \mathcal{P}_{V^\perp} T(U)$$

$$(4.2) \quad = \beta_1 (-\mathcal{P}_V T(U)) + \beta_2 (I - \mathcal{P}_V) T(U),$$

where β_1 and β_2 represent positive relaxation constants. For simplicity, we set $\beta_1 = \beta_2 = \beta$, and can obtain a modified direction, resulting in a modified gradient-type dynamic,

$$(4.3) \quad \beta^{-1} \dot{U} = (I - 2\mathcal{P}_V) T(U).$$

The key to escaping from the basin is to determine the ascent subspace V . Since the minimum eigenvalue is zero in the nullspace-preserving neighbourhood of the GLM $U^{(0)}$, minimizing the Rayleigh quotient $\langle \mathbf{v}, H(U) \mathbf{v} \rangle / \langle \mathbf{v}, \mathbf{v} \rangle$ directly cannot obtain the eigenvector with the smallest positive eigenvalue. We consider an approximate replacement of the nullspace of U by the nullspace of $U^{(0)}$, and impose a constraint condition $\mathbf{v} \perp \mathcal{W}^k(U^{(0)})$. Then the ascent direction $\mathbf{v} \in V$ can be obtained by (4.4).

$$(4.4) \quad \min_{\mathbf{v}} \langle \mathbf{v}, H(U) \mathbf{v} \rangle \quad \text{s.t.} \quad \begin{cases} \langle \mathbf{v}, \mathbf{v} \rangle = 1, \\ \mathbf{v} \perp \mathcal{W}^k(U^{(0)}). \end{cases}$$

We propose a lemma to show the feasibility of obtaining the ascent space by (4.4).

LEMMA 4.1. For any state U in the nullspace-preserving neighbourhood of $U^{(0)}$, the minimum positive eigenvalue of $H(U)$ can be obtained by the optimization problem (4.4).

Proof. Let $\mathcal{W}^k(U^{(0)}) = \text{span}\{\mathbf{v}_{0,1}^k, \mathbf{v}_{0,2}^k, \dots, \mathbf{v}_{0,l_k}^k\}$, where $\{\mathbf{v}_{0,i}^k\}_{i=1}^{l_k}$ are unit orthogonal bases of $\mathcal{W}^k(U^{(0)})$. For a state U in the nullspace-preserving neighbourhood of $U^{(0)}$, there is

$$(4.5) \quad \mathbb{R}^M = \mathcal{W}^k(U) \oplus \mathcal{W}^s(U),$$

where $\mathcal{W}^k(U)$, $\mathcal{W}^s(U)$ can be spanned by unit orthogonal eigenvectors $\{\mathbf{v}_i^k\}_{i=1}^{l_k}$, $\{\mathbf{v}_i^s\}_{i=1}^{l_s}$, respectively.

We replace $\mathcal{W}^k(U)$ by $\mathcal{W}^k(U^{(0)})$, then $\mathbb{R}^M = \mathcal{W}^k(U^{(0)}) \oplus \mathcal{W}^s(U)$. Now, for any $\mathbf{v} \in \mathbb{R}^M$ satisfying $\langle \mathbf{v}, \mathbf{v} \rangle = 1$ and $\mathbf{v} \perp \mathcal{W}^k(U^{(0)})$, we can conclude that $\mathbf{v} \in \mathcal{W}^s(U)$,

$$\mathbf{v} = c_1 \mathbf{v}_1^s + \cdots + c_{l_s} \mathbf{v}_{l_s}^s,$$

where $c_1^2 + \cdots + c_{l_s}^2 = 1$.

Let $\{\lambda_i^s\}_{i=1}^{l_s}$ be eigenvalues corresponding to basis vectors $\{\mathbf{v}_i^s\}_{i=1}^{l_s}$, then

$$\langle \mathbf{v}, H(U) \mathbf{v} \rangle = c_1^2 \lambda_1^s + c_2^2 \lambda_2^s + \cdots + c_{l_s}^2 \lambda_{l_s}^s.$$

Without loss of generality, let λ_1^s be the minimum positive eigenvalue, then

$$\langle \mathbf{v}, H(U) \mathbf{v} \rangle \geq (c_1^2 + \cdots + c_{l_s}^2) \lambda_1^s = \lambda_1^s.$$

Then, λ_1^s represents the minimum of $\langle \mathbf{v}, H(U) \mathbf{v} \rangle$, and when $\mathbf{v} = \mathbf{v}_1^s$, the minimum positive eigenvalue can be obtained. \square

By solving the constrained optimization problem (4.4), we can find the eigenvector that corresponds to the smallest positive eigenvalue, and spans the ascent subspace V . There are various methods for solving the optimization problem (4.4), such as LOBPCG, and gradient-type dynamics. In this case, we use gradient-type dynamics,

$$(4.6) \quad \begin{cases} \gamma^{-1} \dot{\mathbf{v}} = -H(U) \mathbf{v} + \langle \mathbf{v}, H(U) \mathbf{v} \rangle \mathbf{v} + 2 \sum_{i=1}^{l_k} \langle \mathbf{v}_{0,i}^k, H(U) \mathbf{v} \rangle \mathbf{v}_{0,i}^k, \\ \mathbf{v} = \mathbf{v} / \|\mathbf{v}\|_{\ell^2}. \end{cases}$$

where $\gamma > 0$ is a relaxation parameter.

Therefore, we can obtain the ascent direction corresponding to the smallest positive eigenvalue in the nullspace-preserving neighbourhood of $U^{(0)}$ by (4.6), as shown in Figure 4.(a). When U lies outside the nullspace-preserving neighbourhood of the GLM, the nullspace may differ from the nullspace of the GLM, i.e., $\mathcal{W}^k(U) \neq \mathcal{W}^k(U^{(0)})$. However, U remains within the GQR of the GLM, where the Hessian has only zero and positive eigenvalues, indicating the presence of only ascending and translationally invariant directions. As shown in Figure 4(b), the vector \mathbf{v} is perpendicular to $\mathcal{W}^k(U^{(0)})$ and has a component $\bar{\mathbf{v}}$ orthogonal to $\mathcal{W}^k(U)$. When $\mathcal{W}^k(U) \cap \mathcal{W}^k(U^{(0)}) \neq \{\mathbf{0}\}$, an ascent direction $\bar{\mathbf{v}}$ can still be obtained by forcing $\mathbf{v} \perp \mathcal{W}^k(U^{(0)})$.

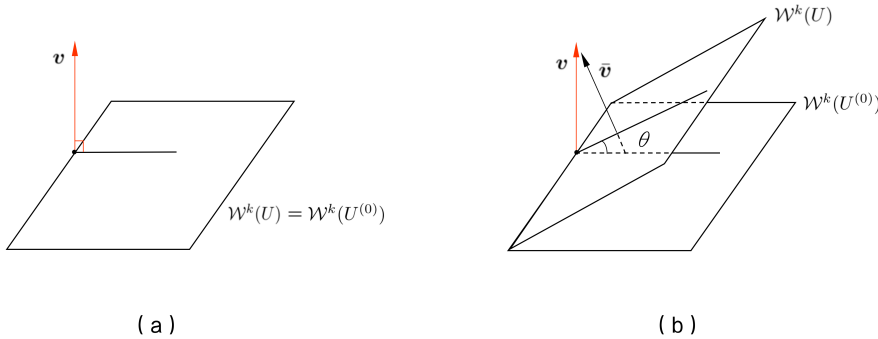


FIG. 4. Schematic diagram of the ascent direction relative to nullspace on MEP. (a). The ascent direction in nullspace-preserving neighbourhood. (b). The ascent direction in the GQR.

4.2. Stage II : Search for index-1 GSP. Once the minimum positive eigenvalue of $H(U)$ becomes negative, meaning that U escapes the GQR of the GLM. We span the ascent space V by the eigenvector \mathbf{v} corresponding to the minimum eigenvalue. Then, to search the index-1 GSP, we only need to find a local maximum on the linear manifold $U + V$, and a local minimum on $U + V^\perp$. Thus the minimax optimization problem of finding index-1 GSP is

$$(4.7) \quad \min_{U^d \in V^\perp} \max_{U^a \in V} E(U^d + U^a),$$

where U^a , U^d are projections of U on V and V^\perp . Many methods can solve this problem, such as Newton method, and gradient-type dynamics. The latter can be written as

$$(4.8) \quad \beta^{-1} \dot{U} = (I - 2\mathcal{P}_V)T(U).$$

Furthermore, the subspace $V = \text{span}\{\mathbf{v}\}$ can be obtained by directly minimizing the Rayleigh quotient,

$$(4.9) \quad \min_{\mathbf{v}} \langle \mathbf{v}, H(U)\mathbf{v} \rangle \quad \text{s.t.} \quad \langle \mathbf{v}, \mathbf{v} \rangle = 1.$$

The dynamic form is

$$(4.10) \quad \begin{cases} \gamma^{-1} \dot{\mathbf{v}} = -H(U)\mathbf{v} + \langle \mathbf{v}, H(U)\mathbf{v} \rangle \mathbf{v}, \\ \mathbf{v} = \mathbf{v} / \|\mathbf{v}\|_{\ell^2}. \end{cases}$$

Algorithm 4.1 summarizes the NPSS method.

Algorithm 4.1 NPSS method

Stage I : Escape from the basin

Input : $U^{(0)} \in \mathbb{R}^M$, $\mathcal{W}^k(U^{(0)}) \subset \mathbb{R}^M$, $\mathbf{v}^{(0)} \in \mathbb{R}^M$ satisfying $\mathbf{v}^{(0)} \perp \mathcal{W}^k(U^{(0)})$

Set $n = 1$, $U^{(n)} = U^{(0)} + \xi \mathbf{v}^{(0)}$, compute $f^{(n)} = T(U^{(n)})$

repeat

Update $U^{(n+1)}$ as (4.3)

Calculate $\mathbf{v}^{(n+1)}$ as (4.6)

$f^{(n+1)} = T(U^{(n+1)})$

$n := n + 1$

If $\langle \mathbf{v}^{(n)}, H(U^{(n)})\mathbf{v}^{(n)} \rangle < \epsilon_\lambda$

Output: the IP $U^{(n)}$

until $\langle \mathbf{v}^{(n)}, H(U^{(n)})\mathbf{v}^{(n)} \rangle < 0$

Output : $U^{(n)}$, the gradient $f^{(n)}$ and the ascent direction $\mathbf{v}^{(n)}$

Stage II : Search for index-1 GSP

repeat

Update $U^{(n+1)}$ as (4.8)

Calculate $\mathbf{v}^{(n+1)}$ as (4.10)

$f^{(n+1)} = T(U^{(n+1)})$

$n := n + 1$;

until $\|f^{n+1}\|_{\ell^2} < \epsilon_f$

Output: the index-1 GSP $U^{(n+1)}$

5. Numerical examples. In this section, to study phase transitions with translational invariance, we apply the NPSS method to search for index-1 GSPs and the gradient descent (GD) method to find the GLM. Several numerical experiments based on LB and LP models are presented: (i). Nucleation from DIS to ordered phases (see Subsection 5.1); (ii). Phase transitions between crystals (see Subsection 5.2); (iii). Phase transitions between quasicrystal and crystal (see Subsection 5.3). Furthermore, in comparison with the HiSD method, we demonstrate the efficiency and reliability of the NPSS method in Subsection 5.3.

For these experiments, we use $[0, 2\pi L)^2$ in 2D and $[0, 2\pi L)^3$ in 3D as the computational domains, and N spatial discretization points in each dimension. All methods are implemented in C++ programming language and run on the same workstation, 12th Gen Intel (R) Core (TM) i7-12700KF, memory 16 GB, under Linux.

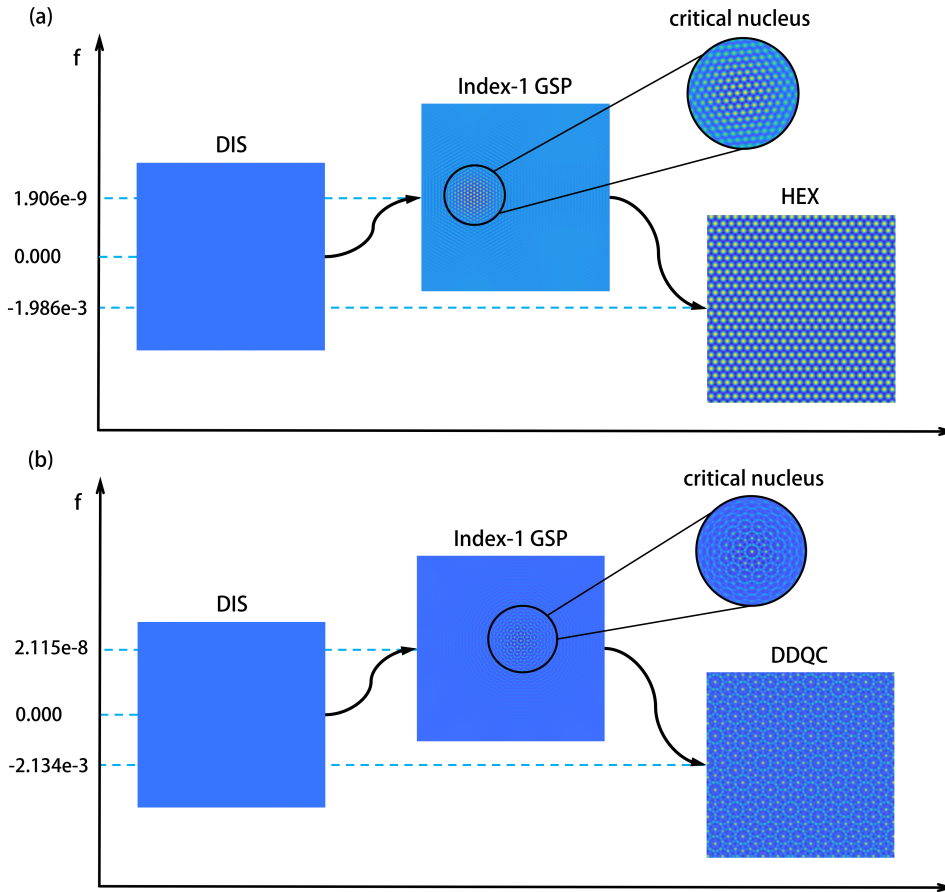


FIG. 5. (a). Transition path from DIS to HEX computed by the NPSS method in LB model with $\tau = 0.001$, $\gamma = 0.5$, where $L = 60$, $N = 900$. (b). Transition path from DIS to DDQC computed by the NPSS method in LP model with $\varepsilon = -0.01$, $\alpha = 0.95$, where $L = 112$, $N = 1024$.

5.1. Nucleation from disordered phases. In this subsection, we use the NPSS method to study the nucleations of the crystal and quasicrystal from DIS. The Hessian of DIS has non-zero eigenvalues, thus the NPSS method only needs to climb along the eigenvector direction corresponding to one positive eigenvalue. We

show phase transition paths from DIS to HEX using the LB model and to DDQC within the LP model (see Figure 5), demonstrating the power of the NPSS method.

5.2. Phase transition between crystals. For the LB model, we compute the phase transition between LAM and HEX using the NPSS method. At $\tau = -0.2$ and $\gamma = 0.28$, LAM is a metastable state with $f = -4.037\text{e-}2$, while HEX is a stable state with $f = -4.158\text{e-}2$. As shown in Figure 6, a circular critical nucleus of HEX with $f = -4.036\text{e-}2$ is found in the transition path from LAM to HEX. A Similar phenomenon has also been obtained by the string method [17].

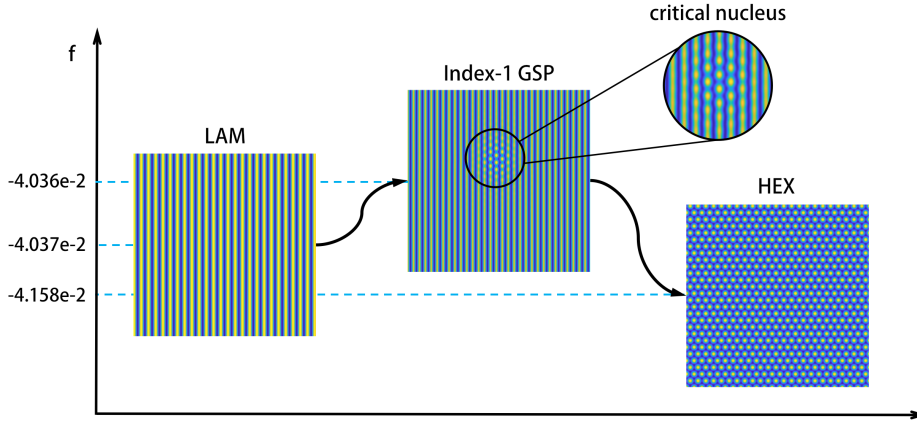


FIG. 6. Transition path from LAM to HEX computed by the NPSS method in the LB model with $\tau = -0.2$, $\gamma = 0.28$, where $L = 60$, $N = 900$.

We also use the NPSS method to study 3D ordered phase transitions and locate the transition state in the LB model. At $\tau = -0.008$ and $\gamma = 0.7$, we study the phase transition from HEX with $f = -1.0514\text{e-}2$ to BCC with $f = -1.2260\text{e-}2$. The complete transition path is shown in Figure 7. From the insert images, the columnar structures in HEX partially deform to form a critical nucleus with $f = -1.0513\text{e-}2$ and eventually evolve into the BCC spherical structure. This result is consistent with the experimental observation [30].

5.3. Phase transition between quasicrystals and crystals. We apply the NPSS method to study the phase transition between DDQC and HEX based on the LP model and compare the computational efficiency with the HiSD method. Let $L = 112$, $N = 1024$, and the termination condition be $\|F(U)\|_{\ell_2} < 1\text{e-}7$. We choose $U^* = U^{(0)} + \xi \mathbf{v}$ as the initial position to search for saddle points, where $U^{(0)}$ is a metastable state that can be obtained by the gradient flow with a proper initial value [14]. \mathbf{v} is usually set as the normalized eigenvector of the smallest positive eigenvalue, which can be computed by the locally optimal block preconditioned conjugate gradient (LOBPCG) method [16]. ξ is a positive constant used to push the system away from the minimum. Table 2 gives the specific values used in this experiment.

Using the NPSS, we obtain a two-stage phase transition from HEX to DDQC, and an inverse phase transition from DDQC to HEX, as shown in Figure 8. These phase transitions have been also simulated in [39].

Taking the phase transition from DDQC to HEX as an example, we use the HiSD method to search for the index-1 GSP from the same starting position U^* with

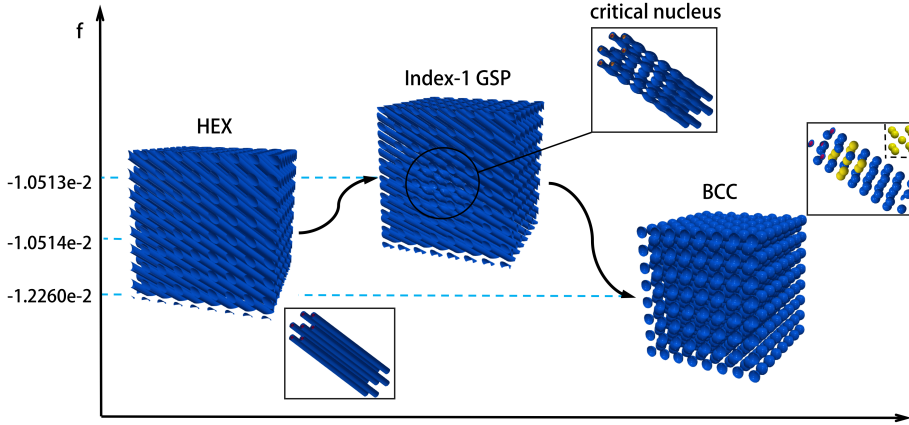


FIG. 7. Phase transition from 3-dimensional HEX to BCC computed by the NPSS method in the LB model with $\tau = -0.008$, $\gamma = 0.7$, where $L = 20\sqrt{2}$ and $N = 224$. Three insert images show the local structures along the body diagonal line.

TABLE 2

The perturbation ξ at the initial position during saddle point search for different phase transition.

stage	DDQC \rightarrow LQ	LQ \rightarrow HEX	HEX \rightarrow LQ	LQ \rightarrow DDQC
ξ	0.1	0.15	0.01	0.1

the same discrete format. Figure 9(a) is a schematic diagram to realize the phase transition process from DDQC to HEX, where HiSD and NPSS methods are applied to search for index-1 GSP. Compared with the NPSS, which directly converges to the index-1 GSP in the upward search stage, the HiSD first converges to the index-2, and index-4 GSPs (see Figure 9(b) and (c)), then requires a downward search to locate the index-1 GSP [39].

We compare the CPU times of both methods when searching for index-1 GSPs. As indicated in Table 3, the NPSS method is more efficient when searching for index-1 GSPs compared to the HiSD method. On average time in the upward search part, the HiSD method takes 3 ~ 5 times longer than the NPSS method, depending on the dimension of the ascent space. Specifically, the HiSD method constructs and updates a $(l_k + 1)$ -dimensional ascent space $V = \text{span}\{\mathbf{v}_{0,1}^k, \dots, \mathbf{v}_{0,l_k}^k, \mathbf{v}\}$, where $\{\mathbf{v}_{0,i}^k\}_{i=1}^{l_k}$ are eigenvectors of zero eigenvalues of $H(U^{(0)})$, and \mathbf{v} is a ascent direction. However, only the ascent direction \mathbf{v} works for escape from the basin. In contrast, the NPSS method directly provides a way to obtain \mathbf{v} , and only needs to update a 1-dimensional ascent space. Moreover, the HiSD method may converge to an index- s GSP ($1 < s \leq l_k + 1$), and must take more time to search down to the index-1 GSP.

6. Discussion. In this section, we investigate the relationship between symmetry-breaking and nullspaces during the phase transition. Considering the phase transition from HEX to LQ in Figure 8(a), we study the structural changes on MEP. There is an IP on MEP, where the smallest positive eigenvalue becomes negative. As shown in Figure 10, before reaching the IP, the structure like state A on the MEP is not obviously different from that of HEX. At the IP, the cylinders transform into the polygonal shape, as shown in (d). After passing the IP, a new cluster gradually ap-

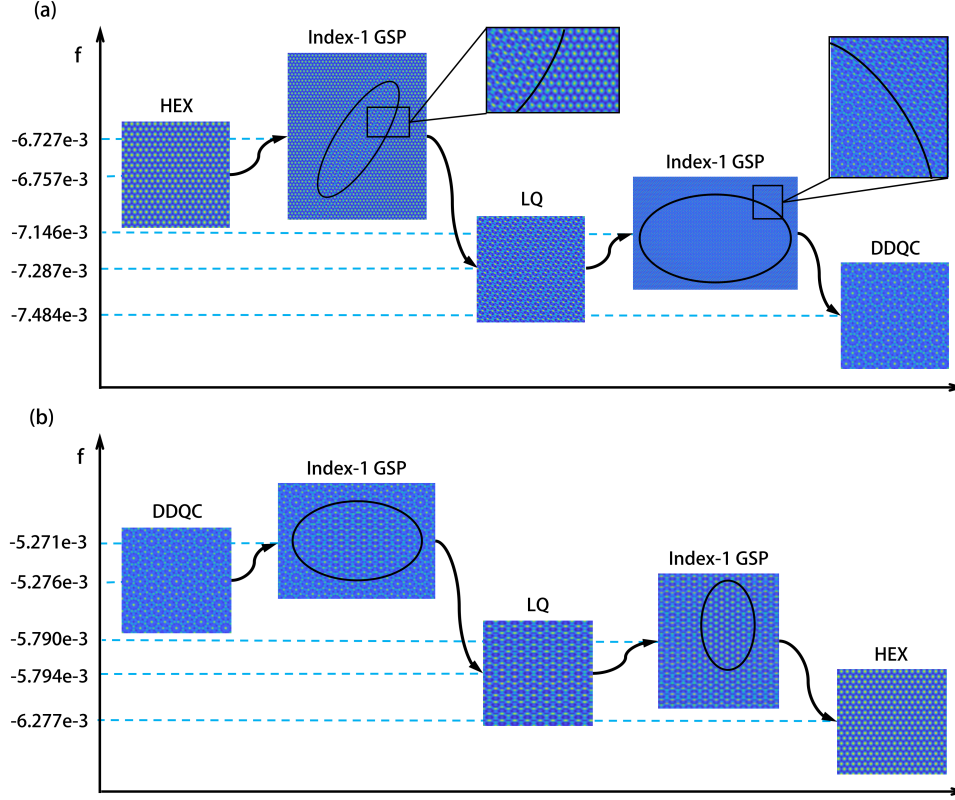


FIG. 8. (a). Two-stage transition path from HEX to DDQC computed by the NPSS method in the LP model with $\varepsilon = 5 \times 10^{-6}$, $\alpha = \sqrt{2}/2$. (b). Two-stage transition path from DDQC to HEX computed by the NPSS method in the LP model with $\varepsilon = 0.05$, $\alpha = 1$.

TABLE 3

Comparison of the computational efficiency of the HiSD and NPSS methods when index-1 GSPs are searched from different initial states. US (DS) represents the upward (downward) search parts, respectively. Times, Iter, and Average time mean total CPU time, sum of iteration steps, and average CPU time per step, respectively.

Initial state	Method	Convergence state	Times/s	Iter	Average time/s
DDQC	NPSS	US: index-1 GSP	4014	16240	0.25
	HiSD	US: index-2 GSP	21435	17230	1.24
		DS: index-1 GSP	888	4370	0.20
LQ	NPSS	US: index-1 GSP	3334	14460	0.23
	HiSD	US: index-4 GSP	3805	4030	0.70
		DS: index-1 GSP	2643	8150	0.32

pears until the critical nucleus is formed, as shown in (e) and (f), respectively. It can be seen that the IP is the critical point where the symmetry-breaking begins to occur. Subsection 3.1 has shown that the translational invariance of the stable state U is related to the dimension of the nullspace $\mathcal{W}^k(U)$. Does the invariance of the ordered structure before the IP on MEP also correspond mathematically to the invariance of the nullspace? A natural question is whether the states on the MEP before the IP can maintain the nullspace invariance.

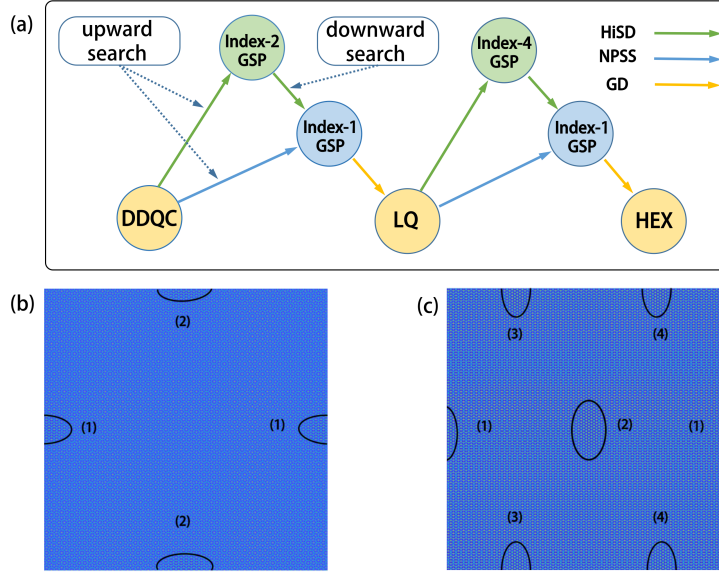


FIG. 9. (a). Illustration of transition path searched by HiSD and NPSS method. (b). Index-2 GSP searched by HiSD method from DDQC. (c). Index-4 GSP searched by HiSD method from LQ.

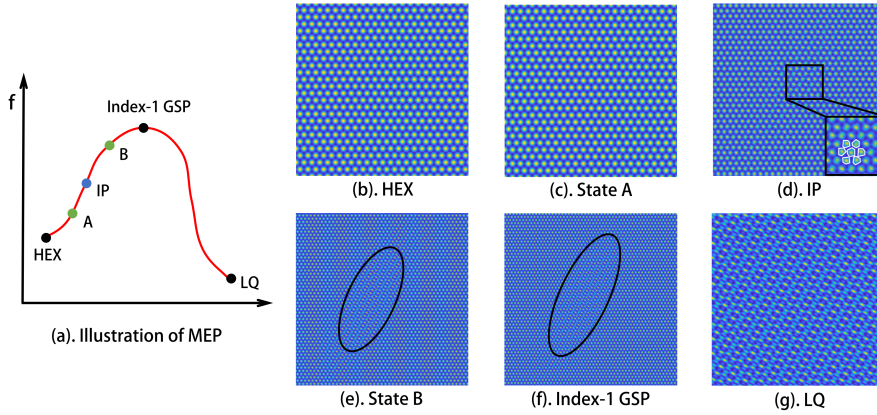


FIG. 10. (a). Illustration of the MEP from HEX to LQ. (b)-(g). Several states on MEP marked in (a), where A and B are two intermediate states before and after reaching the IP, respectively.

To further explore the property of nullspace invariance on the MEP, we introduce some notations and definitions below. We generate a sequence of states $\{U^{(j)}\}_{j=0}^n$ on MEP from GLM to index-1 GSP by the GD method, where $U^{(0)}$, $U^{(m)}$ and $U^{(n)}$ ($0 < m < n$) represent the GLM, IP and index-1 GSP, respectively. Then we calculate the smallest six eigenvalues of $H(U^{(j)})$, $j = 1, 2, \dots, n$, and their corresponding eigenvectors by the LOBPCG. We rewrite $\mathcal{W}^k(U^{(0)}) = \text{span}\{\mathbf{v}_{0,1}^k, \dots, \mathbf{v}_{0,l_k}^k\}$. \mathbf{v} is one of eigenvectors on the MEP. We define a angle θ to measure relations between \mathbf{v} and

$\mathcal{W}^k(U^{(0)})$ as

$$\theta = \arccos(\|\mathbf{v}_p\|_{\ell^2} / \|\mathbf{v}\|_{\ell^2}),$$

$$\mathbf{v}_p = \sum_{i=1}^{i=l_k} \frac{\langle \mathbf{v}, \mathbf{v}_{0,i}^k \rangle}{\langle \mathbf{v}_{0,i}^k, \mathbf{v}_{0,i}^k \rangle} \mathbf{v}_{0,i}^k,$$

where \mathbf{v}_p is the projection of \mathbf{v} in $\mathcal{W}^k(U^{(0)})$.

Then we study properties of nullspaces $\{\mathcal{W}^k(U^{(j)})\}_{j=0}^n$ by exploring smallest six eigenvalues $\{\lambda_i\}_{i=1}^6$ and angles $\{\theta_i\}_{i=1}^6$ between corresponding eigenvectors and $\mathcal{W}^k(U^{(0)})$. Figure 11 (a) illustrates the variation curves of the six smallest eigenvalues from the GLM to the index-1 GSP. From $U^{(0)}$ to the neighborhood of the IP, $|\lambda_1|$ and $|\lambda_2|$ remain below $\epsilon_0 = 1e-10$, which can be considered as zero eigenvalues. This means that the dimension of nullspaces along the MEP before reaching the neighborhood of the IP is equal to that of the GLM. As shown in Figure 11 (b), θ_1 and θ_2 are close to zero before reaching the neighbourhood of IP, indicating that the nullspace on the MEP belongs to $\mathcal{W}^k(U^{(0)})$ in this part of the MEP. In summary, the nullspace of the state on the MEP from the GLM to the neighborhood of the IP is approximately equal to the nullspace of the GLM, consistent with the structural invariance of the parent phase during the phase transition from the GLM to the IP.

We refer to this feature as the *nullspace-preserving* property, and surmise that symmetry preservation implies nullspace preservation in phase transitions with translational invariance. The IP on the MEP corresponds mathematically to the dividing point where the nullspace is no longer preserved, and physically to the critical point where the symmetry begins to change.

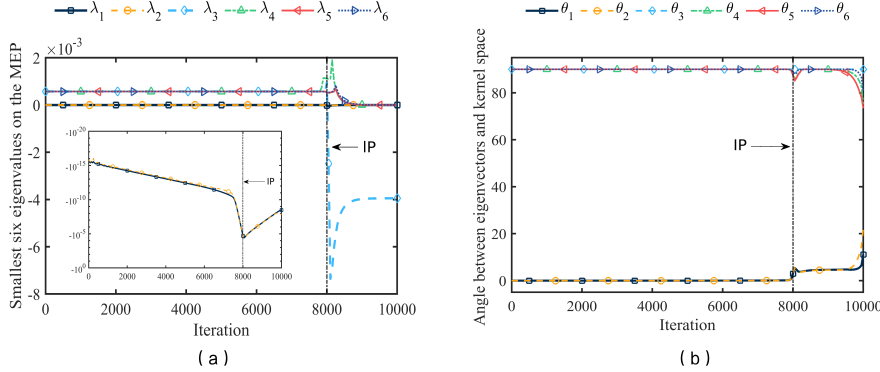


FIG. 11. (a). Variation of the smallest six eigenvalues on the MEP from HEX to the index-1 GSP. The subgraph shows the variation details of λ_1 and λ_2 . (b). Angles $\{\theta_i\}_{i=1}^6$ between the nullspace of HEX and the eigenvectors corresponding to the smallest six eigenvalues on the MEP.

7. Conclusion. In this paper, we develop the NPSS method to study phase transitions with translational invariance based on the LB and LP models. The NPSS method can ensure that the search direction is always ascending by making it perpendicular to the nullspace of the metastable state. We employ the NPSS method to study the nucleation and phase transition between quasicrystal and crystal, and between crystals. Results show that the NPSS method can locate index-1 GSPs with an economical computational amount compared with HiSD, and can efficiently reveal transition paths between ordered structures with translational invariance. In

particular, we identify an important critical point, the IP, on the MEP associated with symmetry-breaking. Before reaching the IP, we find that the nullspaces on the MEP have the *nullspace-preserving* property. In the future, we plan to apply the NPSS method to more interesting phase transition problems and to improve it with problem-dependent features.

REFERENCES

- [1] S. BRAZOVSKII, *Phase transition of an isotropic system to a nonuniform state*, Soviet Journal of Experimental and Theoretical Physics, 41 (1975), p. 85.
- [2] D. CAO, J. SHEN, AND J. XU, *Computing interface with quasiperiodicity*, Journal of Computational Physics, 424 (2021), p. 109863.
- [3] Y. CAO, V. FATEMI, S. FANG, K. WATANABE, T. TANIGUCHI, E. KAXIRAS, AND P. JARILLO-HERRERO, *Unconventional superconductivity in magic-angle graphene superlattices*, Nature, 556 (2018), pp. 43–50.
- [4] M. F. CARILLI, K. T. DELANEY, AND G. H. FREDRICKSON, *Truncation-based energy weighting string method for efficiently resolving small energy barriers*, Journal of Chemical Physics, 143 (2015), p. 054105.
- [5] R. COWLEY, *Structural phase transitions i. landau theory*, Advances in Physics, 29 (1980), pp. 1–110.
- [6] G. CUI, K. JIANG, AND J. Z. Y. CHEN, *Finding minimum energy pathways*, submitted, (2023).
- [7] W. E, W. REN, AND E. VANDEN-EIJNDEN, *String method for the study of rare events*, Physical Review B, 66 (2002), p. 052301.
- [8] W. E AND X. ZHOU, *The gentlest ascent dynamics*, Nonlinearity, 24 (2011), p. 1831.
- [9] S. GU AND X. ZHOU, *Simplified gentlest ascent dynamics for saddle points in non-gradient systems*, Chaos: An Interdisciplinary Journal of Nonlinear Science, 28 (2018), p. 123106.
- [10] G. HENKELMAN AND H. JÓNSSON, *Improved tangent estimate in the nudged elastic band method for finding minimum energy paths and saddle points*, Journal of Chemical Physics, 113 (2000), pp. 9978–9985.
- [11] G. HENKELMAN AND H. JÓNSSON, *A dimer method for finding saddle points on high dimensional potential surfaces using only first derivatives*, Journal of Chemical Physics, 111 (1999), pp. 7010–7022.
- [12] G. HENKELMAN, B. P. UBERUAGA, AND H. JÓNSSON, *A climbing image nudged elastic band method for finding saddle points and minimum energy paths*, Journal of Chemical Physics, 113 (2000), pp. 9901–9904.
- [13] K. JIANG, W. SI, AND J. XU, *Tilt grain boundaries of hexagonal structures: A spectral viewpoint*, SIAM Journal on Applied Mathematics, 82 (2022), pp. 1267–1286.
- [14] K. JIANG, J. TONG, P. ZHANG, AND A.-C. SHI, *Stability of two-dimensional soft quasicrystals in systems with two length scales*, Physical Review E, 92 (2015), p. 042159.
- [15] H. JÓNSSON, G. MILLS, AND K. W. JACOBSEN, *Nudged elastic band method for finding minimum energy paths of transitions*, in Classical and quantum dynamics in condensed phase simulations, World Scientific, 1998, pp. 385–404.
- [16] A. V. KNYAZEV, *Toward the optimal preconditioned eigensolver: Locally optimal block preconditioned conjugate gradient method*, SIAM Journal on Scientific Computing, 23 (2001), pp. 517–541.
- [17] T. LI, P. ZHANG, AND W. ZHANG, *Nucleation rate calculation for the phase transition of diblock copolymers under stochastic cahn–hilliard dynamics*, Multiscale Modeling & Simulation, 11 (2013), pp. 385–409.
- [18] R. LIFSHITZ AND H. DIAMANT, *Soft quasicrystals—why are they stable?*, Philosophical Magazine, 87 (2007), pp. 3021–3030.
- [19] R. LIFSHITZ AND D. M. PETRICH, *Theoretical model for faraday waves with multiple-frequency forcing*, Physical Review Letters, 79 (1997), pp. 1261–1264.
- [20] D. MCCLENAGAN, *Landau theory of complex ordered phases*, master’s thesis, McMaster University, 2019.
- [21] H. MH, *Differential equations, dynamical systems, and linear algebra*, Pure and Applied Mathematics, 5 (1974).
- [22] R. MIRON AND K. A. FICHTHORN, *The step and slide method for finding saddle points on multidimensional potential surfaces*, Journal of Chemical Physics, 115 (2001), pp. 8742–8747.
- [23] B. NAGYFALUSI, L. UDVARDI, AND L. SZUNYOGH, *Magnetic ground state of supported*

- monatomic fe chains from first principles*, Journal of Physics: Condensed Matter, 34 (2022), p. 395803.
- [24] N. PROVATAS AND K. ELDER, *Phase-field methods in materials science and engineering*, John Wiley & Sons, 2011.
 - [25] W. REN AND E. VANDEN-EIJNDEN, *A climbing string method for saddle point search*, Journal of Chemical Physics, 138 (2013), p. 134105.
 - [26] A. SAMANTA AND W. E, *Optimization-based string method for finding minimum energy path*, Communications in Computational Physics, 14 (2013), p. 265–275.
 - [27] D. SHECHTMAN, I. BLECH, D. GRATIAS, AND J. W. CAHN, *Metallic phase with long-range orientational order and no translational symmetry*, Physical Review Letters, 53 (1984), p. 1951.
 - [28] A.-C. SHI, J. NOOLANDI, AND R. C. DESAI, *Theory of anisotropic fluctuations in ordered block copolymer phases*, Macromolecules, 29 (1996), pp. 6487–6504.
 - [29] S. V. SMAALEN, *Incommensurate crystal structures*, Crystallography Reviews, 4 (1995), pp. 79–202.
 - [30] N. SOTA, K. SAIJO, H. HASEGAWA, T. HASHIMOTO, Y. AMEMIYA, AND K. ITO, *Directed self-assembly of block copolymers into twin bcc-sphere: phase transition process from aligned hex-cylinder to bcc-sphere induced by a temperature jump between the two equilibrium phases*, Macromolecules, 46 (2013), pp. 2298–2316.
 - [31] E. STEIN, J. W. MILNOR, M. SPIVAK, R. WELLS, R. WELLS, AND J. N. MATHER, *Morse theory*, no. 51, Princeton University Press, 1963.
 - [32] A. SUTTON AND R. BALLUFFI, *Interfaces in crystalline materials*, Oxford University Press, 1995.
 - [33] J. SWIFT AND P. C. HOHENBERG, *Hydrodynamic fluctuations at the convective instability*, Physical Review A, 15 (1977), p. 319.
 - [34] P. TOLEDANO AND J.-C. TOLEDANO, *The Landau theory of phase transitions : application to structural, incommensurate, magnetic, and liquid crystal systems*, vol. 3, World Scientific Publishing Company, 1987.
 - [35] A.-P. TSAI, J. GUO, E. ABE, H. TAKAKURA, AND T. J. SATO, *A stable binary quasicrystal*, Nature, 408 (2000), pp. 537–538.
 - [36] C. WANG, K. JIANG, P. ZHANG, AND A.-C. SHI, *Origin of epitaxies between ordered phases of block copolymers*, Soft Matter, 7 (2011), pp. 10552–10555.
 - [37] J. XU, C. WANG, A.-C. SHI, AND P. ZHANG, *Computing optimal interfacial structure of modulated phases*, Communications in Computational Physics, 21 (2017), p. 1–15.
 - [38] X. YAO, J. XU, AND L. ZHANG, *Transition pathways in cylinder-gyroid interface*, Communications in Computational Physics, 32 (2022), pp. 810–828.
 - [39] J. YIN, K. JIANG, A.-C. SHI, P. ZHANG, AND L. ZHANG, *Transition pathways connecting crystals and quasicrystals*, Proceedings of the National Academy of Sciences, 118 (2021), p. e2106230118.
 - [40] J. YIN, Y. WANG, J. Z. CHEN, P. ZHANG, AND L. ZHANG, *Construction of a pathway map on a complicated energy landscape*, Physical Review Letters, 124 (2020), p. 090601.
 - [41] J. YIN, L. ZHANG, AND P. ZHANG, *High-index optimization-based shrinking dimer method for finding high-index saddle points*, SIAM Journal on Scientific Computing, 41 (2019), pp. A3576–A3595.
 - [42] J. ZHANG AND Q. DU, *Shrinking dimer dynamics and its applications to saddle point search*, SIAM Journal on Numerical Analysis, 50 (2012), pp. 1899–1921.
 - [43] P. ZHANG AND X. ZHANG, *An efficient numerical method of landau-brazovskii model*, Journal of Computational Physics, 227 (2008), pp. 5859–5870.